

Wind loading on a stepped roof building: comparison of field measurements, wind tunnel data, and standard provisions

M. Aldoum^{1*}, T. Stathopoulos¹, M. Chavez², A. Baskaran²

1- Department of Building, Civil and Environmental Engineering, Concordia University, Montreal, Quebec, Canada

2- National Research Council of Canada, Ottawa, Ontario, Canada

* Corresponding author: muradaldoum@gmail.com

Abstract

This study investigates wind loads on stepped roof buildings measured in the field and in an atmospheric boundary layer wind tunnel to verify the suitability of the North American codes and standards for the design of stepped roofs. Good agreement has been generally found between field and wind tunnel results. The field measurements and wind tunnel results were compared with the NBCC 2020 and ASCE 7-22 provisions. It was found that the Edge provisions of NBCC 2020 are currently underestimated and need to be increased. The study suggests merging the Corner and Edge zones into a single “Perimeter” zone in NBCC 2020 as this would resolve the current underestimation of the NBCC Edge wind loads and add simplicity to the Code provisions. Peaks of ASCE 7-22 were found conservative, except for the zone near the step wall on the lower roof; ASCE 7-22 positive peaks seem to be underestimated.

Keywords: Stepped roof building; Wind loads; Wind tunnel; Field data; NBCC 2020; ASCE 7-22

1 Introduction

NBCC 2020 and ASCE 7-22 give directions and guidance for the design of cladding and secondary components of buildings with multi-level flat roofs. The design of such buildings basically emanates from

two studies (Stathopoulos and Luchian, 1990; Stathopoulos and Luchian, 1991). The two studies investigated wind loads of flat stepped roof buildings experimentally in 1990 and 1991. The first study focused on L-shaped stepped roofs, and Stathopoulos and Luchian (1991) examined wind loads on U-shaped stepped roof buildings. Considering modern equipment and devices for measuring wind pressures in wind tunnels and the availability of limited full-scale data obtained by the National Research Council of Canada (NRCC), a verification of the Canadian code provisions and the American standard guidelines of stepped roof buildings could be made.

The sole difference between the design of a flat roof building and a stepped roof building in NBCC 2020 is the positive pressure-gust coefficients recommended for the zone of the lower roof near the step wall; this zone should be designed based on the positive pressures recommended for walls. The American standard, ASCE 7, had similar design guidelines in the previous version, ASCE 7-16; however, the stepped roof design guidelines have been updated in the recent version, ASCE 7-22; the positive pressures of the lower roof-step wall interaction are now referenced to the flat roof design guidelines.

Stathopoulos and Zhou (1993) studied wind loads on a stepped roof numerically; the numerical results were compared with Stathopoulos and Luchian (1990). A good agreement was found in the mean pressure coefficients for normal wind direction. Cao et al. (2012) investigated wind loads on medium-rise buildings with multi-level roofs using a large model (length scale: 1/67) and compared their results with ASCE 7-10. The area-averaged peak coefficients evaluated by Cao et al. (2012) agree with ASCE7-10 for large tributary areas; however, the experimental area-averaged peaks associated with small tributary areas were much higher than ASCE 7-10 peaks.

In the current study, a full-scale wind loading investigation on a stepped roof building was conducted by the National Research Council of Canada (NRC) in collaboration with Special Interest Group on Dynamic Evaluation of Roofing Systems (SIGDERS) consortium. The full-scale stepped roof building is in Woodstock city, Ontario; the building is a branch for Soprema Inc.; it is equipped with 15 pressure taps on the upper and lower roofs. Fig. 1 shows the location of the building and the upstream exposure near the

building, it also shows a photo of the full-scale building, the instrumented zones are marked by the red dashed square and lines. field data was scanned in 2021, from June to December. In addition, a model of the full-scale building was tested in the atmospheric boundary layer wind tunnel of Concordia University. The wind tunnel model has a length scale of 1:400; the total number of roof pressure taps is 180; 132 taps on the lower roof and 48 taps on the upper roof.

In the present study, the field and experimental results were compared with the corresponding provisions and design guidelines in NBCC 2020 and ASCE 7-22. The two sources, field and wind tunnel, provide a considerable approach to verify the wind provisions in codes and standards. The same approach was used by Chavez et al. (2022) to verify the suitability of Figure 4.1.7.6.-C in NBCC 2020. It is anticipated that the outcomes of this paper would contribute to the discussion of whether the provisions and design guidelines of the stepped roof buildings in the North American codes and standards should be revised.

2 Field measurements

The ultimate objective of this study is to compare the field measurements with the wind tunnel results and the design provisions and guidelines in the North American codes and standards for stepped roof buildings. Measurement of wind loads on a building in the field is burdensome; the complex structure of the real wind flow due to the selected building, surroundings, and the topographical details near the building make the quantification of the field wind pressures challenging. To ensure a fair comparison with the Canadian code and the American standard, the building was selected based on the shape (stepped roof building) indicated in the target figures in NBCC 2020 and ASCE 7-22.

2.1 Building Selection and Instrumentation

The selected full-scale building is a branch for Soprema Inc. in Woodstock City, Ontario, Canada. This commercial building is a fair representation of a stepped roof as defined in the provisions. The type of terrain around the building within a radius of about 300 m (984 ft) can be described as an open country

with minimal obstructions. The exposure changes to light suburban at a distance of about 300 m (984 ft) on the western side of the full-scale building. An escarpment near the building and a few structures and equipment (e.g., silos) on the North-West (315°) side of the building may slightly alter the approaching wind from that direction.

The external wind load is continuously monitored by 15 pressure taps (PT) strategically installed on the roof to cover critical roof zones on the lower and upper levels. Each sensor is composed of a ¼-inch (6.35 mm) OD and 12-inch (0.3 m) long copper tube which is inserted through the entire roof assembly at the locations shown in Fig. 2. The external end of the taps is bent to prevent water intrusion, while the internal end is connected to a dedicated differential pressure transducer via a ¼-inch (6.35 mm) ID plastic tubing. The length of the plastic tube linking the copper tube to the transducer is kept as short as possible (12 to 24 inches (0.3 to 0.6 m)) to minimize external pressure distortions.

The corresponding local wind speed -and wind direction- is needed to calculate the external pressure coefficient. The location of wind speed measurements is considered as one of the challenges of field data measurements from “in-service” buildings. In most of the field studies, an anemometer is located farther from the monitored building to avoid building-induced interferences. In the current study, due to the nature of the building and operational constraints, that option was not possible and the wind tower with the anemometer was installed on the roof of the building – see Fig. 3. An ultrasonic anemometer was attached to the top of a 5 m (16 ft) tall wind tower (equivalent to 13.6 m (44 ft) from the ground which is 1.6 times the height of the lower-level roof) and it is placed near the centre of the roof at approx. 23 m (75 ft) from the building edge to limit the effects of the flow separation at the building edges. The influence of the building on the wind speed reading was not investigated; however, it can be expected that the building may reduce the approaching wind speed (and increase the turbulence) at the anemometer location which may affect the pressure coefficients. The side-by-side comparison with wind tunnel simulations permits to overcome this uncertainty of the field data.

A reference pressure (P_r) is needed as an input at each differential pressure transducer. As discussed for the wind speed measurements, P_r is also a challenging parameter, particularly for studies on “in-service” buildings. Ideally, P_r should be as stable as possible and independent of the influence of the building. In field studies, the most common practice to get a reliable P_r is from an underground box that is located far from the building. In the current study that approach was not possible; instead, P_r was measured inside the building in a storage room without windows and/or openings to ensure a relatively stable reference pressure. P_r was measured inside a 12" (304 mm) height and 4" (102 mm) diameter copper cylinder which is vented to the building interior (storage room). Then P_r is connected to every pressure transducer via long ¼-inch (6.35 mm) OD plastic tubing to ensure that all the transducers share the same reference pressure.

The wind speed (and wind direction) and the corresponding pressure at every pressure tap were continuously recorded at a rate of 100 Hz in a custom data acquisition system (DAQ) for further analysis. Additional details regarding the instrumentation (pressure sensors, local wind speed and direction), DAQ, and data analysis can be found in Chavez et al. 2022.

Fig. 4 shows the elevation, plan, and pressure tap layout of the full-scale building. The building has a step height (h_1) of 3.4 m, lower roof height (h_2) and upper roof height (H) of 8.6 m and 12 m, respectively. The pressure zones of NBCC 2020 and ASCE 7-22 are shown on the building plan, where z and b , were determined based on NBCC 2020. For b , it is one and a half of the step height (h_1), and z was governed by the building heights.

2.2 Data Processing

Data collection in the field was started in June 2021 and ended in December 2021. The collected data were first filtered by extracting 10-minute records with a peak wind speed of 13.4 m/s (30 mph) or higher, in other words, when a peak wind speed of greater or equal to 13.4 m/s (30 mph), a 10-minute record is selected by extracting the data 5 minutes before and after the occurrence of the peak wind speed. It should be mentioned that wind speed and direction can significantly fluctuate within the 10-minute record;

however, it can be assumed that at high speed the fluctuations are reduced and wind tends to be more stable. The segmentation criterion based on the 13.4 m/s (30 mph) wind speed peak threshold aimed to maximize the stability of the data within the 10 minutes. This segmentation process is combined with a manual stationarity check where the segments containing spikes or sudden changes in wind direction or wind speed are discarded; this approach was adopted by Chavez et al. 2022 as the first filter of the field data. This approach was also used in previous NRC studies (Baskaran et al., 2012; Bartko et al., 2016; Martins et al., 2016; Baskaran et al., 2018; Chavez et al., 2020). The second filter is based on the average wind speed of the 10-minute record; it was decided to include only records with an average wind speed greater or equal to 6.3 m/s (14 mph). Again, the two filters were adopted to ensure that the selected field records are with high wind speed, consequently, it would ensure relatively stable wind records; this resulted in 253 10-minute records selected for analysis in this study. It should be mentioned that all records included in Chavez et. al. (2022) have mean wind speeds equal to or higher than 8 m/s (18 mph). Fig. 5 shows a plot of the mean wind speeds and the turbulence intensities of the selected records. It can be observed that records with the highest wind speeds are associated with low turbulence intensities.

The selected 10-minute records are then classified considering the predominant wind direction, which is determined for each 10-minute record based on the average of the wind directions recorded during the 10 minutes; then the records are grouped into certain wind directions with a tolerance of $\pm 11.25^\circ$. For example, records with predominant wind direction ranges from 258.75° to 281.25° are labeled as wind emanating from West (270°). Fig. 6 shows the building plan aligned to the compass wind directions and the number of 10-minute records linked to each wind direction; 7 wind directions were eventually considered, and the largest number of records happened to be grouped to WNW (292.5°) with 127 records. The rest of the records are distributed among wind directions ranging from SSW (202.5°) to NNW (337.5°).

2.3 Pressure coefficient calculations

The selected 10-minute records include the time series of pressure fluctuations of each pressure tap and the wind speed. The purpose of the field measurements is to compare the field wind loads with the Canadian code and the American standard; NBCC 2020 and ASCE 7-22 provide the wind-speed-independent pressure coefficients for design of buildings. Therefore, the field pressures need to be transformed and quantified in pressure coefficients.

The pressure coefficient at instant t within the 10 minutes is calculated as follows:

$$C_p(t) = \frac{P(t) - P_{ref}(t)}{\frac{1}{2}\rho V_{ref}^2} \quad (1)$$

Where:

$C_p(t)$ is the pressure coefficient calculated at instant t ,

$P(t)$ and $P_{ref}(t)$ are the field external and reference pressures measured at instant t ,

V_{ref} is the mean wind speed of the 10-minute record, and

ρ is the air density.

The reference pressure should be as stable as possible and not affected by the wind and building interaction. As done in previous studies (Chavez et al., 2022 and 2020), it was decided to read the reference pressure inside the building in a small storage room without windows and no circulation. This location is a practical solution to minimize external wind effects, the variability of temperature and relative humidity, and then ensure the stability of the reference pressure.

Three types of field pressure coefficients will be presented in this study: mean pressure coefficients and positive and negative peak pressure coefficients. The mean pressure coefficient is the average of the pressure coefficients $C_p(t)$ in the 10-minute record. For the negative peak pressure coefficient, the 10-

minute record is divided into ten equal segments, and the minimum value in each is considered to obtain 10 minima; The average of the 10 values represents the negative peak $C_p(t)$. The same steps apply to calculate the positive peak $C_p(t)$ by considering the maximum of each segment.

3 Concordia wind tunnel experiment

Measurement of wind loads in wind tunnels overcomes the limitations encountered in the field as wind tunnels allow scanning wind pressures over experimental models for all wind directions, unlike the field measurements which depend on the natural wind that blows from limited directions as shown in Fig. 6. Also, installing pressure taps in an existing building is expensive and complicated. In contrast, experimental models can be equipped with high-density of pressure taps to obtain a higher resolution of pressures scanned on the surfaces of the model. To overcome the field limitations, a model of the full-scale building was tested in a wind tunnel.

The model testing was conducted in the Atmospheric Boundary Layer Wind Tunnel of Concordia University for an open country exposure. The model was constructed using a length scale of 1:400, with the full-scale plan dimensions of 138.5 m x 58.9 m (454 ft x 193 ft); the heights of the upper and lower roofs are 12 m (39.4 ft) and 8.6 m (28.2 ft), respectively. Fig. 7 shows the elevation, plan, and pressure tap layouts of the model. The roof includes a total of 180 pressure taps: 132 taps on the lower roof, and 48 on the upper level. In addition, 10 pressure taps were installed in the wall at the step (Wall 1) and lower roof wall (Wall 2). Fig. 8 shows photos of the model in the wind tunnel. The model was tested in the wind tunnel with and without surroundings; the results of both tests are comparable with a difference of less than 5 % in the most-critical peaks, and using either test leads to the same conclusion. It was decided to include the experimental wind measurements for the isolated model, without surroundings, since it extends the results for the stepped roof buildings in general rather than a special case with certain obstructions around the building. The wind speed was measured at the wind tunnel using a 4-hole cobra probe at a frequency of 1000 Hz for 32 seconds.

Fig. 9 presents wind speed and turbulence intensity profiles of the wind tunnel flow, ESDU ($z_0 = 0.03 \text{ m}$), and the power law, all profiles are normalized with respect to the upper roof height, $H = 12 \text{ m}$ (39.4 ft). The wind tunnel wind speed profile fits the power law for an exponent of 0.16 and has a good agreement with ESDU. Also, the turbulence intensity profiles of the wind tunnel flow and the ESDU are comparable. Fig. 10 presents a comparison between the wind tunnel power spectrum and the analytical spectrum of Von Karman; the wind spectra are in good agreement. The length scale of turbulence was estimated to be 74 m at the upper roof height.

ASCE 49-21 requires the Reynolds number to be greater than 11,000 for wind tunnel simulation. Considering the upper roof height as a characteristic length, the Reynolds number is 17,000, which satisfies the ASCE 49-21.

For the wind tunnel, the wind pressures were scanned in the wind tunnel over each pressure tap at a frequency of 300 Hz for wind azimuth range from 0° - 360° at a step of 10° . The pressure records were then used to evaluate mean, positive peak, and negative peak pressure coefficients. All pressure coefficients represent the scanned pressures normalized by the dynamic pressure at the respective roof height. Peaks were estimated by fitting the extreme measured pressures using the Gumbel distribution; the peak is selected based on 80% fractile level of the fitted peaks. This approach is different from using the average of 10 peaks for the estimation of the field peaks; however, the difference between the two approaches is relatively small.

4 Results

This section compares local and area-averaged pressure coefficients of the field and wind tunnel; in addition, results from Stathopoulos and Luchian (1990) were included in the comparison. The local pressure coefficients are presented for selected taps on edge, corner, and middle zones on upper and lower roofs. Also, the enveloped area-averaged positive and negative peaks of the wind tunnel and field were calculated for several tributary areas in the roof pressure zones of the lower and upper roofs; the area-

averaged peaks are used to compare the experimental and field results with the stepped roof provisions in the Canadian code and ASCE 7-22.

4.1 Field versus Wind tunnel Data

This subsection presents a comparison of local pressure coefficients between the field and Concordia wind tunnel (WT) with respect to wind direction.

Field and Concordia mean and negative peak pressure coefficients at selected taps in the lower and upper roofs are compared in Fig. 11. The taps were selected to represent all zones as follows: tap 1 from the lower roof corner zone, tap 5 from the lower roof edge zone, tap 7 from the lower roof interior zone, and tap 13 from the upper roof edge. Concordia pressure coefficients are presented in blue and represent wind direction range from 0° - 360° with an increment of 10° . For the field, the solid black line represents the average pressure coefficient of the 10-minute records at each of the 7 wind directions: SSW (202.5°), SW (225°), WSW (247.5°), W (270°), WNW (292.5°), NW (315°), NNW (337.5°). In addition to the field average pressure coefficient, the maximum and minimum pressure coefficients are included for each wind direction. It should be noted that Concordia and field pressure coefficients in this subsection are different with respect to the averaging time of mean wind speed; Concordia mean wind speed corresponds to one hour in the full-scale, and 10 minutes were used for the field mean wind speed. Field pressure coefficients were not converted to correspond to one hour since the difference is 10% only (Durst, 1960).

The comparison in Fig. 11 shows agreement in the mean and negative peak pressure coefficients between the two sources for wind directions ranging from SSW (202.5°) to WNW(292.5°); however, except for the mean pressure coefficients of tap 7, noticeable discrepancies in the mean and negative peak pressure coefficients between the field and Concordia are observed for NW (315°) and NNW (337.5°) in which field pressure coefficients are always higher in magnitude than the pressure coefficients of Concordia. Nevertheless, the azimuthal change of pressure coefficients of field and Concordia follows almost the same trend. The highest wind tunnel negative peaks of tap 1 were recorded around WSW (247.5°) and 280° with

a value of -6 and the field peak is almost the same for WSW (247.5°). For edge taps, 5 and 13 (both located on the edge), the field and Concordia mean, and negative peaks compare in the same way in which the agreement and the gap between the black and the blue lines are almost similar. However, Concordia pressure coefficients are slightly higher in magnitude for the upper edge. Tap 7 is in the interior zone of the lower roof which is a flow reattachment zone or at least associated with low turbulent wind flow which explains the agreement of the mean pressure coefficients.

The discrepancies can probably be attributed to the difference in the structure of the approaching wind flow due to the increased turbulence in the field which ranges from about 15% to 45% as shown in Fig. 5, compared to the stable 18% in the wind tunnel. In addition, the wind upstream exposure would also contribute to the differences between the field and the wind tunnel; the field building is bounded by an escarpment alongside the North-West edge, which certainly explains the differences between pressure coefficients of the field and Concordia for NW and NNW. Furthermore, the variability of wind direction in the field may also contribute to the discrepancies presented in Fig. 11. It is worth mentioning that past studies showed that reproducing the fluctuating pressure in wind tunnel testing is difficult (Tieleman, 2003); therefore, the presented discrepancies are anticipated.

Taps 8-11 are located on the lower roof near the step, this zone is usually subjected to relatively high positive pressures, and NBCC 2020, as mentioned previously, recommends design positive peaks higher than those for a roof without a step, therefore, it was decided to name this zone as the positive pressure zone in this paper and compare the positive pressure for taps 8-11. Fig. 12 compares the field and Concordia positive peak pressure coefficients in the positive pressure zone. Field and Concordia pressure coefficients were plotted using the same approach explained for Fig. 11. For the four taps, field and Concordia positive peaks are comparable except for those plotted for SSW (202.5°); it should be noted that field pressure coefficients of SSW (202.5°) represent only two 10-minute records which may explain the disagreement between field and Concordia for SSW (202.5°). For NW (315°) and NNW (337.5°), the field positive peaks are slightly higher than those of Concordia which is probably attributed to the presence of the escarpment

near the building as discussed above. For the rest of the wind directions, Concordia positive peaks are marginally higher than those of the field. It should be mentioned that the positive peaks reported by the field of taps outside the positive pressure zone are close to zero, therefore, it was decided to include the positive peak of taps 8, 9, 10, and 11 only.

In summary, the pressure coefficients of the field and the wind tunnel are comparable with some discrepancies at some taps; those differences are mainly attributed to the different upstream exposure of the field and wind tunnel, as well as to the higher level of turbulence in the field affecting some particular field records.

4.2 Field versus Concordia versus Stathopoulos and Luchian (1990)

The experimental stepped roof model in Stathopoulos and Luchian (1990) was tested in the boundary layer wind tunnel of Concordia University for simulated open country exposure with a turbulence intensity of about 14% at the lower roof height. The study reported wind loads on several configurations of stepped roof buildings. Among all considered configurations, there is one case with lower and upper roof heights of 10 m (32.8 ft) and 20 m (65.6 ft), respectively, and plan dimensions of 30 m (98.4 ft) by 60 m (196.9 ft); this case was the closest to the stepped roof setup of the current study. It was decided to compare the results of the current study with those of the mentioned case.

Table 1 compares the most critical mean and negative peak pressure coefficients (among all wind directions) between current field, Concordia, and Stathopoulos and Luchian (1990) in the lower corner, edge and interior zones, and the upper edge zone. It should be mentioned that the field pressure coefficients in Table 1 represent the highest value of the black solid line (average) in Fig. 11. Pressure coefficients (means and peaks) of Stathopoulos and Luchian (1990) are lower in magnitude than those from field and Concordia. This is anticipated as the test in Stathopoulos and Luchian (1990) was conducted for lower turbulence intensity at the roof height which resulted in reducing the fluctuating pressures and the overall value of mean pressure coefficients. The field pressure coefficients (mean and peaks) are higher in

magnitude than those of Concordia except for the negative peaks of pressure coefficients of the lower and upper edges. This can be explained by having the most critical peaks occur for wind directions other than those considered in the field. For example, Pressure tap 13 (upper edge, see Fig. 11) has the most critical peak recorded at about 190°.

4.3 Comparison with NBCC 2020

Recommendations of NBCC 2020 for the design of stepped roofs are given in Figure 4.1.7.6.-D. The stepped roof figure in the Canadian code does not include design peaks and refers to the flat roof design peaks given in Figure 4.1.7.6.-C for the design of the upper and lower roof. However, there is an exception for the design positive peaks of the positive pressure zone on the lower roof in which the positive peaks recommended for walls and stipulated in Figure 4.1.7.6.-B should be applied.

Figs. 13, 14, and 15 compare the field, Concordia, and NBCC 2020 local and area-averaged peak pressure coefficients, which are denoted by C_pC_g in the Canadian code, of the lower roof, positive pressure zone, and upper roof, respectively. NBCC 2020 peaks correspond to a wind speed averaged over one hour; similarly, peaks of Concordia correspond to hourly averaged wind speeds at the respective roof height (i.e., the lower roof and the upper roof peaks are normalized with respect to dynamic pressures at the lower roof and upper roof heights, respectively). On the other hand, field peaks are referenced with respect to 10-minute mean wind speed duration. The blue solid lines represent the corresponding design peaks provided by the NBCC 2020, and the red solid circles represent results from Concordia. For field data, the results are plotted using a range rather than a certain single value. The field C_pC_g black squares represent the average obtained by averaging three sets of field data; first, the average C_pC_g was calculated for each wind direction, in other words, the first set includes C_pC_g 's of all records within each wind direction. The second average was taken for the C_pC_g 's sets of taps within each pressure zone for each of the 7 wind directions to obtain a set of 7 C_pC_g values, the third set. The last step is to calculate the statistical parameters of the third set which includes the average, or the third average represented by the black squares in Figs. 13-15,

the standard deviation, and maxima and minima. The thick black line represents the average \pm the standard deviation of the third set. The area-averaged CpCg's of field and Concordia data were calculated for several tributary areas all over the roof to investigate the attenuation of wind pressures when larger areas are considered. It should be mentioned here that the local field and Concordia CpCg are presented in Figs. 13-15 for arbitrarily assumed tributary areas of 0.2 m^2 (2.2 ft^2) and 0.1 m^2 , (1.1 ft^2) respectively. Also, the tributary areas of the field taps were calculated by assuming equal areas associated with the taps in each zone; for example, the lower roof corner zone includes four taps and has dimensions of $3.4 \text{ m} \times 3.4 \text{ m}$ which results in an area of 11.56 m^2 , consequently, the tributary area of one tap in the lower roof corner zone is 2.9 m^2 .

Fig. 13 shows the comparison for the three-roof pressure zones of the lower roof: Corner, Edge, and Interior zones; the positive pressure zone determined by the distance b is excluded from the comparison in Fig. 13. For the corner zone, the average value of negative CpCg's from the field and Concordia are almost equal to the recommendations of NBCC 2020, therefore, it can be concluded that the corner zone provisions need not to be revised. For larger tributary areas in the corner zone, the NBCC 2020 negative peaks curve is below the field and Concordia; however, the calculation of area-averaged pressure coefficients is affected by the density of taps in the considered area, consequently, CpCg's for large areas will not be used to assess the code provisions. For the edge zone, it is evident that the code negative curve is below field and Concordia peaks, and it can be concluded that the code negative peaks recommended for the Edge zone need to be increased. The Interior zone negative peaks of Concordia are stacked above and below the NBCC 2020 curve, on the other hand, the field negative peaks are higher in magnitude than the code; as the agreement of the field and Concordia was not reached, this paper does not pronounce a position regarding any revision for the Interior zone provisions at this time. For the positive peaks, the field, Concordia, and NBCC 2020 are comparable for the Corner, Edge, and Interior zones; therefore, the positive peaks of NBCC 2020 need not be revised. The observations made in Fig. 13 are consistent with the previous

study (Chavez et al., 2022) where field and two wind tunnel experiments were conducted to verify the suitability of the low-slope gabled roof provisions in NBCC.

Fig. 14 shows $C_p C_g$'s of the positive pressure zone near the step wall. The negative peaks of the field data are lower in magnitude than the Code peaks, while Concordia peaks are almost comparable to the code peaks. For the positive peaks, Concordia $C_p C_g$'s are higher than the Code and the field data showed lower $C_p C_g$'s than the Code. Again, the agreement is not reached, and the results of Concordia and field are not conclusive regarding the positive peaks in the positive pressure zone; therefore, there is no evidence to revise the code positive peaks.

Fig. 15 presents the peaks of the upper roof in the Edge and Interior zone; the results of the Corner zone are not presented in this figure because the Corner zone does not include pressure taps in the wind tunnel model and the field building. For the Edge zone, the field and Concordia negative peaks are higher in magnitude than the code specifications, and it can be concluded that the Edge zone provisions need to be increased. It can be seen in Fig. 15 that the comparison of peaks in the Interior zone includes the code and Concordia peaks only, this is so because the roof of the monitored building does not include taps in the interior zone of the upper roof. Nevertheless, Concordia negative peaks roughly agree with the curve of the Code; therefore, no change is required. The positive peaks of Concordia and field measurements are aligned with the Code curve in both zones and consequently, the positive peaks of the Code are conservative.

In summary, based on the results from Concordia and field measurements, the Code negative and positive provisions of Corner and Interior zones are conservative enough, and no changes are suggested. The Edge zone negative peaks provided by the Code are currently underestimated and need to be increased. This conclusion was reached by comparing the findings of the Edge zone of both the lower and upper roofs with the Code. It should be noted that Concordia $C_p C_g$ values of the Corner and Edge zones are comparable with a difference of less than 1. Therefore, this paper would support the recommendation made by Chavez et al. (2022) to merge Edge and Corner zones into a single zone and name it "Perimeter" zone in Figure

4.1.7.6.-C. This would add simplicity to the Code provisions. Simplicity in codification is important to make the construction process easier and reduce the risk of worker errors during construction.

4.4 Comparison with ASCE 7-22

Design guidelines of stepped roof buildings provided by ASCE 7-10 were like those provided by the Canadian code. However, those design guidelines were updated twice in ASCE 7-16 and ASCE 7-22. The first update was implemented in ASCE 7-16 in which the values of peaks were increased based on Kopp and Morrison (2014); however, the pressure zones and positive pressure coefficients of the area of the lower roof near the step wall remained unchanged; those positive pressures were referenced to the wall design peaks like ASCE 7-10. The second update was carried on in the recent edition, ASCE 7-22; the change was done for both roof pressure zones and positive pressure of the lower roof near the step wall. All peaks, including positive peaks, are now referenced to the flat roof design peaks. The roof pressure zones are also like those of the flat roof excluding zone 1'. It should be noted that the positive pressure zone, i.e., the area of the lower roof near the step wall, is governed by the same distance (one and a half of the step wall height) in both ASCE 7-22 and NBCC 2020.

Field and Concordia peaks are compared with ASCE 7-22 in Figs. 16, 17, and 18 for Zone 3, Zone 2, and Zone 1 respectively. Comparison figures in this subsection mimic those in subsection 3.4, for which Zone 3, Zone 2, and Zone 1, correspond to the Corner zone, Edge zone, and Interior zone, respectively. Two modifications were performed herein; field and Concordia peaks were converted based on Durst (1960) to correspond to a 3-second gust duration as is the case for peaks of ASCE 7. In addition, the pressure zones are represented by a different set of taps, for example, pressure tap 4 is in the NBCC Corner zone and Zone 2 based on ASCE 7; however, this was done for a few taps only as the difference between roof pressure zones of NBCC 2020 and ASCE 7-22 is not huge. The methodology used to plot the field peaks is elaborated in subsection 4.3.

Fig. 16 compares peaks for Zone 3, Zone 2, and Zone 1 of the lower roof; the positive pressure zone is excluded. ASCE 7-22 negative peak curves are conservative in the three zones at which peaks of Concordia and the average field peaks are below the ASCE 7-22 peaks. For the positive pressures, Concordia peak average and field peaks are covered by the ASCE 7-22 curves; therefore, the study indicates no revision for the ASCE 7-22 peaks in the three mentioned zones would be necessary.

The positive pressure zone peaks are compared in Fig. 17. ASCE 7-22 negative peaks are conservative; however, the positive peak curve of ASCE 7-22 is underestimated by both Concordia peaks and field peaks. Therefore, the study concludes that the positive peaks of ASCE 7-22 need to be increased. It is suggested to reference the positive pressure peaks of this particular zone to the wall positive peaks as was the case for ASCE 7-16. The wall positive peak is equal to +1 which addresses the underestimation. The comparison of the upper roof peak is shown in Fig. 18. ASCE 7-22 curves are conservative and design peaks need not to be revised.

The study indicated that ASCE 7-22 design peaks are conservative except for the positive pressure peaks of the lower roof zone near the step wall in which ASCE 7-22 peaks are exceeded by the peaks of field results and Concordia. It is suggested to predicate the positive peaks near the step wall to the wall design peaks.

5 Conclusion

The paper presented the wind loads on a stepped roof building measured in the field (full-scale) and the wind tunnel and compared the findings with NBCC 2020 and ASCE 7-22. The objective of the paper is to verify the suitability of the NBCC 2020 and ASCE 7-22 wind load requirements for the design of stepped roof buildings. It was concluded that the C_pC_g 's of the NBCC 2020 are conservative enough except for the negative C_pC_g 's specified for the Edge zone. The field and wind tunnel results indicated that the NBCC 2020 Edge peaks are currently underestimated and need to be increased. The paper suggested merging the Edge and Corner zones in NBCC 2020 into a single zone named "Perimeter". This would resolve the

current underestimation of the Edge wind loads and add simplicity to the Code provisions. Design peaks of ASCE 7-22 were found conservative except for the positive peaks of the zone near the step wall on the lower roof, the study indicated that positive peaks are less than the wind tunnel and field findings and need to be increased. The study suggested referencing the positive peaks of the mentioned zone to those specified for walls in ASCE 7-22.

Acknowledgment

The authors want to thank the following organizations/staffs for their contribution to this project: Jean-Francois Coté, Florent Bellini from SOPREMA for their collaboration with our research project by providing authorization to instrument the plant in Woodstock, ON; and Jason Kirk from SOPREMA for his valuable support during the sensors' installation and assistance with the remote data collection. We would like to thank the BLWTL personnel at Concordia University for their support during testing. NRC technical team efforts (A. Duric, S. K. P. Ko, J. Saragosa, J. Tomkins, and D. Van Reenen) are greatly appreciated. The authors are also grateful to Professor Y. Tominaga of Niigata Institute of Technology for his kind agreement to be Acting Editor for this paper and carry out the review process outside the Editorial Manager System since the Editor of the Journal is a co-author of this paper.

References

ASCE/SEI 7-10, 2010. Minimum Design Loads for Buildings and Other Structures. Structural Engineering Institute of ASCE, Reston, VA.

ASCE/SEI 7-16, 2016. Minimum Design Loads and associated criteria Buildings and Other Structures. Structural Engineering Institute of ASCE, Reston, VA.

ASCE/SEI 7-22, 2022. Minimum Design Loads and associated criteria for Buildings and Other Structures. Structural Engineering Institute of ASCE, Reston, VA.

ASCE/SEI 49-21, 2021. Wind Tunnel Testing for Buildings and Other Structures. Structural Engineering Institute of ASCE, Reston, VA.

Bartko, M., Molleti, S., Baskaran, A. 2016. In situ measurements of wind pressures on low slope membrane roofs. *J. Wind Eng. Ind. Aerodyn* 153, 78–91.

Baskaran, A., Molleti, S., Ko, S., Van Reenen, D. 2012. What is Real? - Field Monitoring the Wind Performance of Commercial Roofs. Proceedings of the RCI, Inc., 27th International Convention & Trade Show, March 15-20, 2012, Dallas, TX, USA.

Baskaran, A., Molleti, S., Martins N., Martín-Pérez, B. 2018. Development of wind load criteria for commercial roof edge metals. *J. Archit. Eng., ASCE*, 24(3).

Cao, J., Tamura, Y., Yoshida, A. 2012. Wind Pressures on Multi-level Flat Roofs of Medium-rise Buildings. *J. W. Eng. Aerodyn.*; 103: 1-15.

Chavez, M., Baskaran, A., Aldoum M., Stathopoulos T., Geleta, T.N., Bitsuamlak, G.T. 2022. Wind loading on a low-slope gabled roof: Comparison of field measurements, wind tunnel data, and code provisions. *Eng. Struct*, 267, 114646.

Chavez, M., Baskaran A., Feng, Ch., Gan Chowdbury, A. 2020. Effect of assembly construction on the wind induced pressure of membrane roofs. *Eng Struct*; 221:110725. <https://doi.org/10.1016/j.engstruct.2020.110725>.

Durst., C.S. 1960. Wind Speeds Over Short Periods of Time. *Meteor. Magazine*, 89, 181-187.

Kopp, G. A., and Morrison, M. J. 2014. Component and cladding pressures and zones for the roofs of low-rise buildings. Boundary Layer Wind Tunnel Report, University of Western Ontario, London, ON.

NBCC 2020. National Building Code of Canada 2020. Issued by the Canadian Commission on Buildings and Fire Codes, National Research Council of Canada.

Martins, N.E., Martin-Perez, B., Baskaran, A., 2016. Application of statistical models to predict roof edge suction based on wind speed. *J. Wind Eng. Ind. Aerodyn.*, 150, 42-53.

Stathopoulos, T., Luchian, H. 1990. Wind Pressures on Buildings with Stepped Roofs. *Can. J. Civ. Eng.*; 17 (4):569–577.

Stathopoulos, T., Luchian, H, 1991. Wind Loads on Flat Roofs with Discontinuities. CSCE Annual Conf., Vancouver.

Stathopoulos, T., Zhou, Y.S., 1993. Numerical simulation of wind-induced pressures on buildings of various geometries. *J. Wind Eng. Ind. Aerodyn.* 46–47 (C), 419–430.

Tieleman, H.W., 2003. Wind tunnel simulation of wind loading on low-rise structures: a review. *J. Wind Eng. Ind. Aerodyn.* 91, 1627–1649.

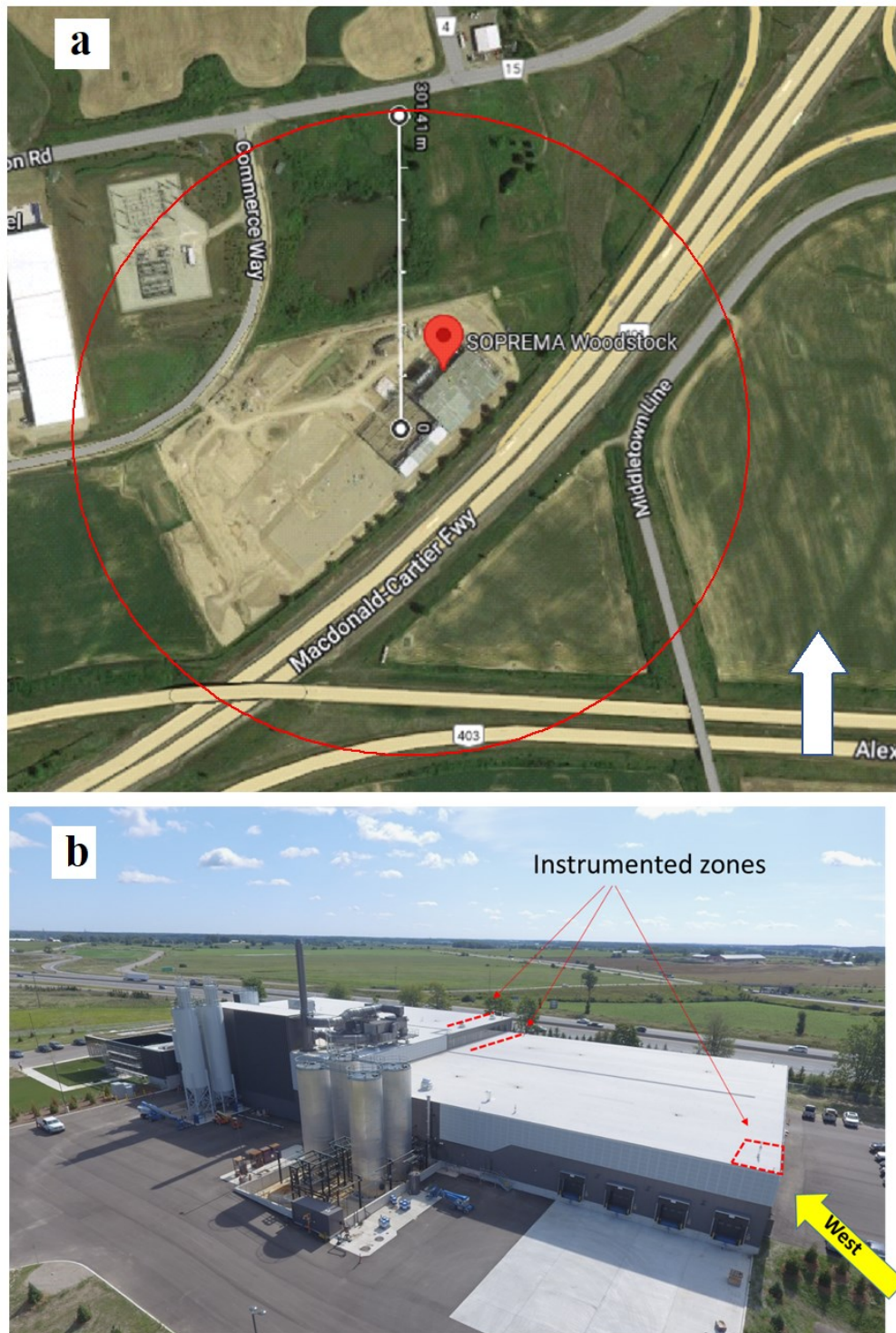


Figure 1:a). Building location (relevant upstream structures within a radius of 300 m), b). Soprema experimental building in Woodstock, Ontario.

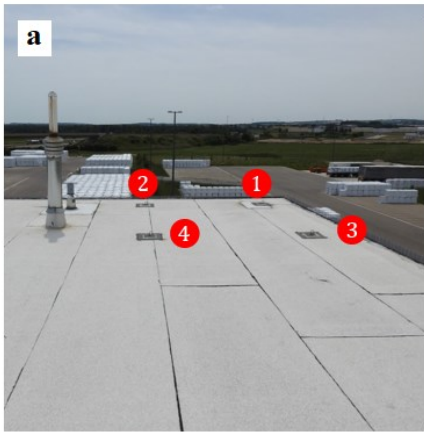
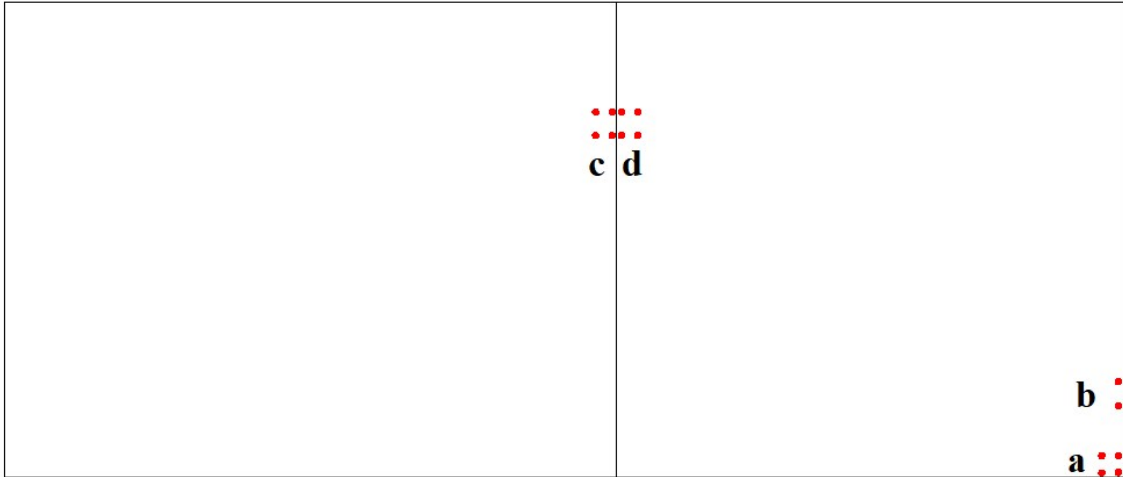



Figure 2: Photos of pressure taps on the lower and upper roofs

Upper roof	Lower roof
	

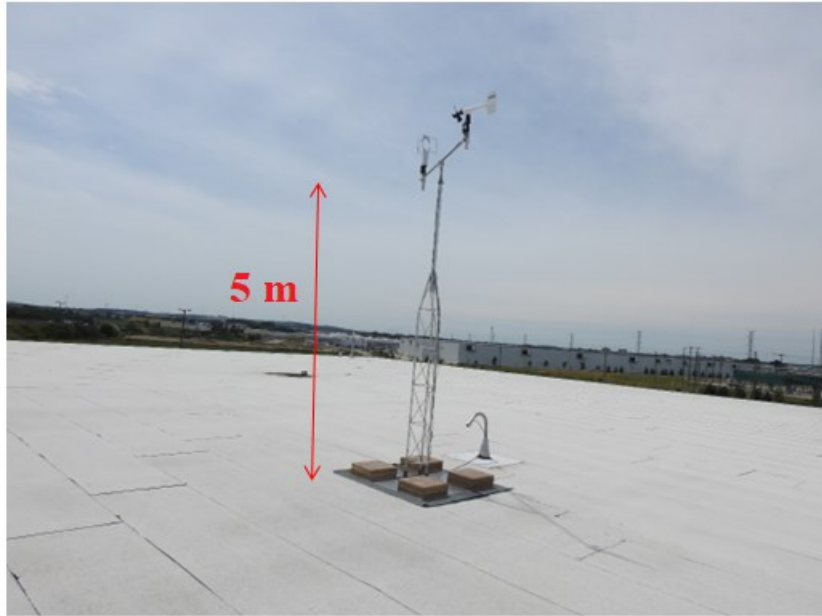


Figure 3: Photo of the anemometer (fixed on the middle of the Lower roof).

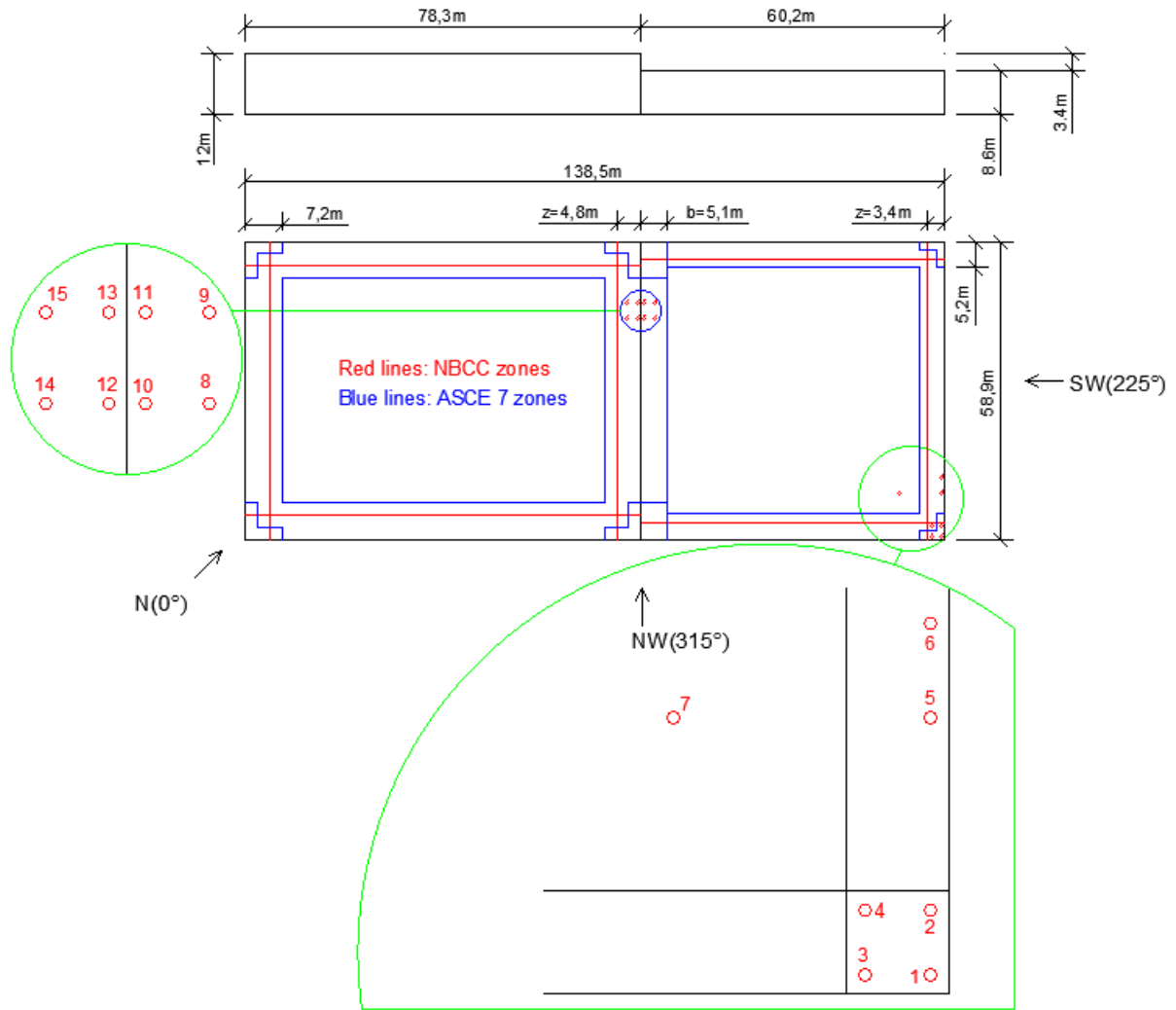


Figure 4: Full-scale building (dimensions in meters).

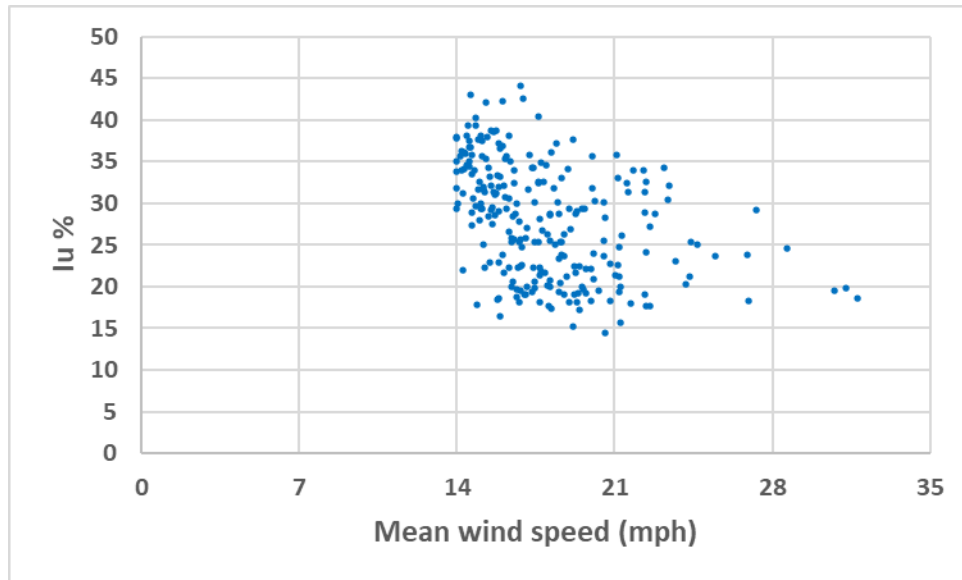


Figure 5: Turbulence intensities (I_u) and mean wind speed of the selected records, 253 records with mean wind velocities greater or equal to 14 mph.

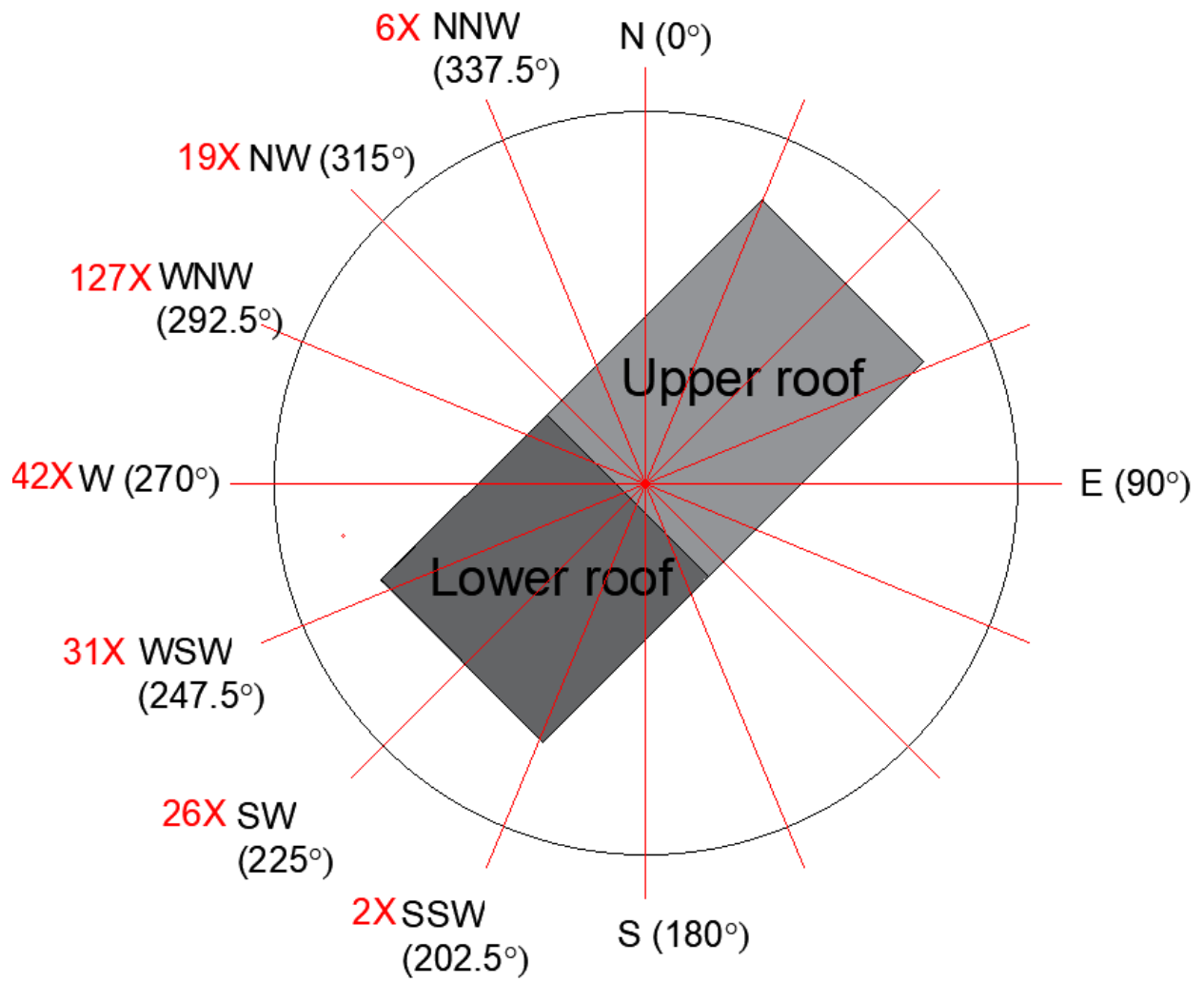


Figure 6: Directional distribution of the 253 records.

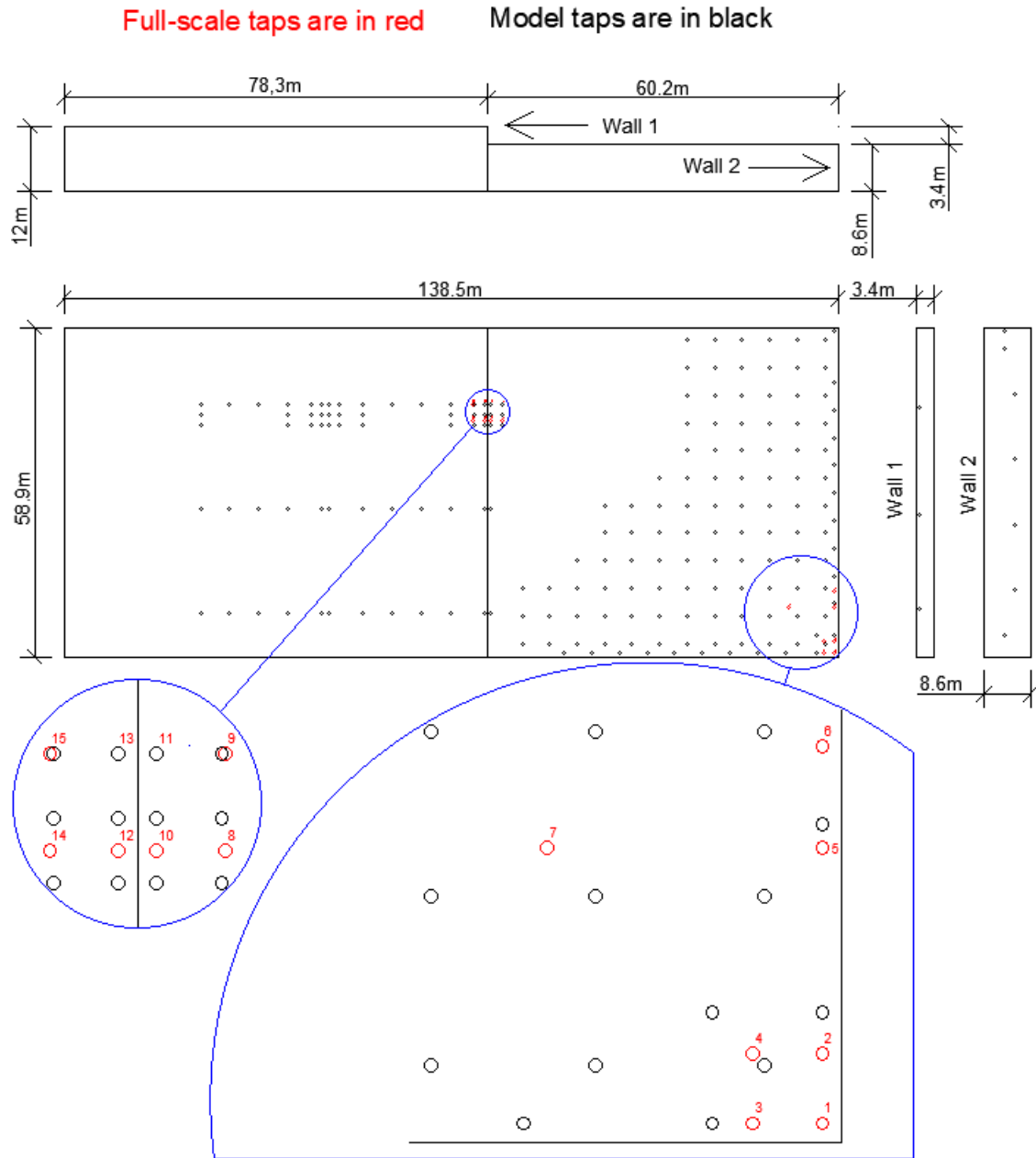


Figure 7: Elevation and plan of the wind tunnel model, dimensions are full-scale (meters), length scale: 1:400.

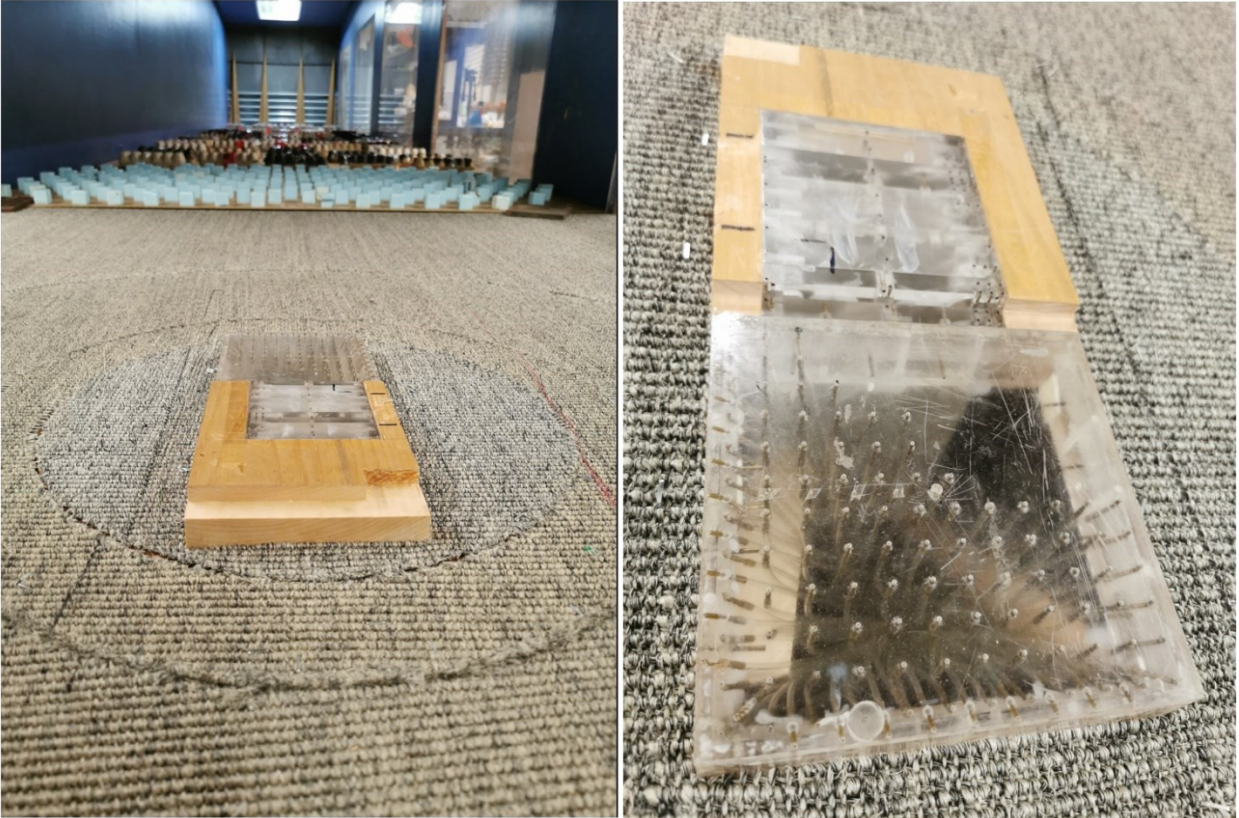


Figure 8: Photos of the model in the wind tunnel (isolated).

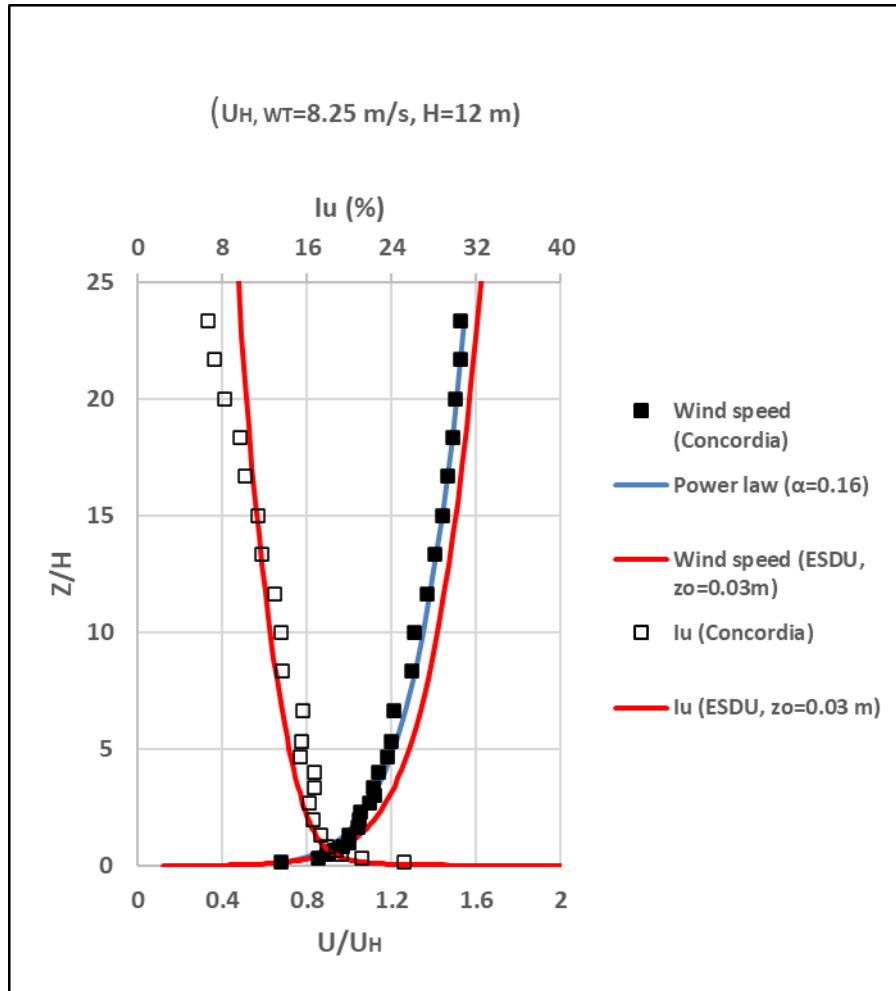


Figure 9: Vertical variation of mean wind speed and longitudinal turbulence intensity of Concordia, ESDU ($z_0 = 0.03 \text{ m}$), and power law for open country terrain.

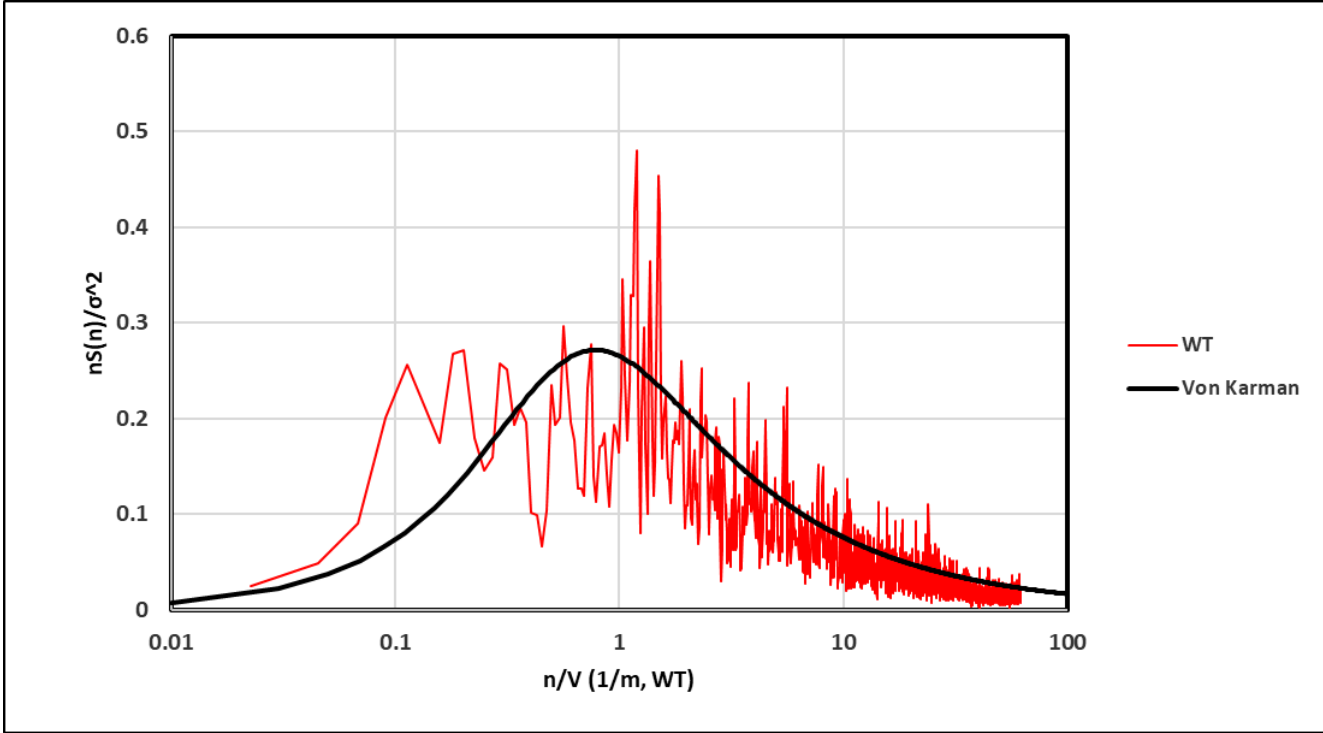


Figure 10: Spectra of wind speed at the upper roof height.

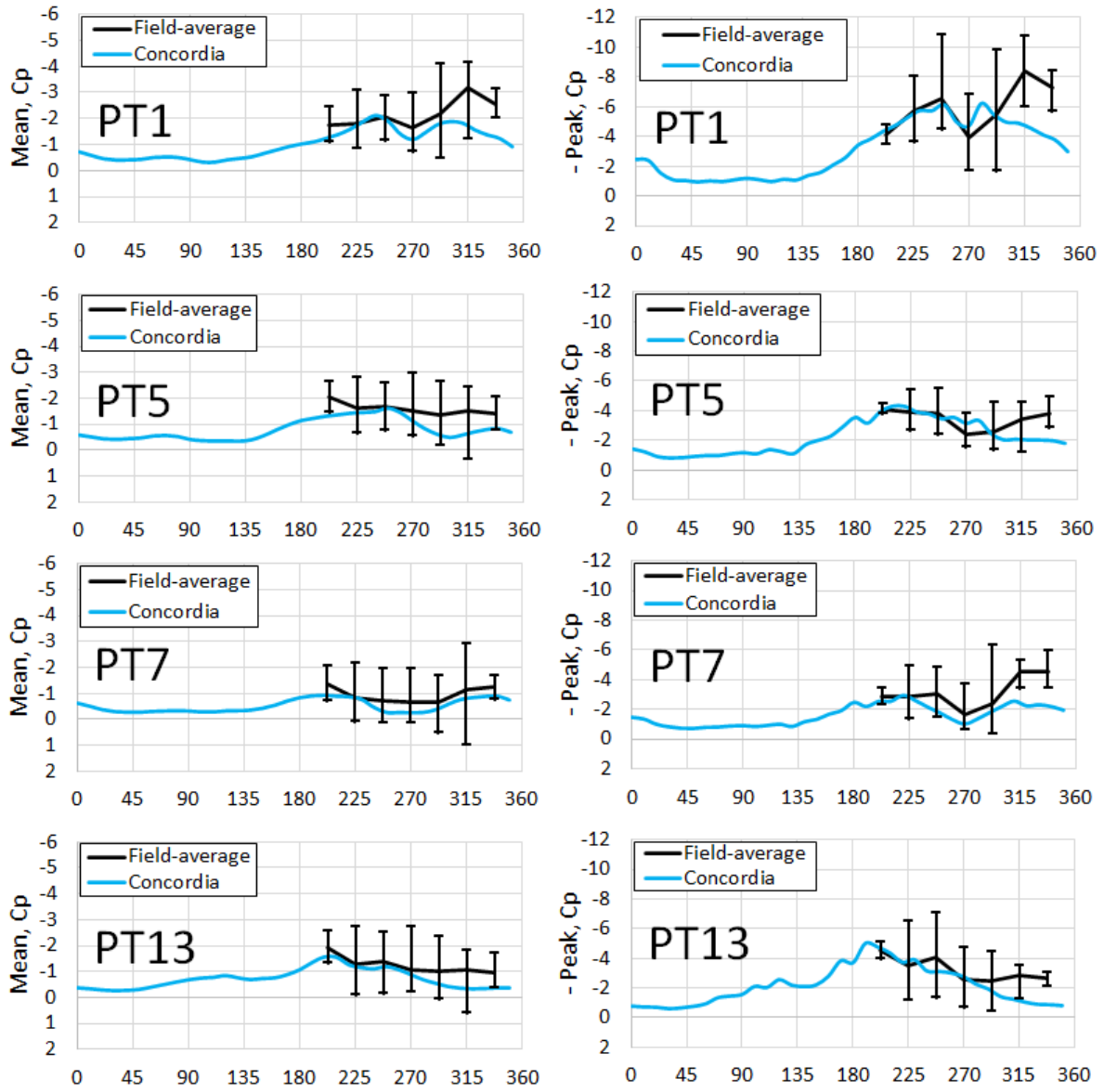
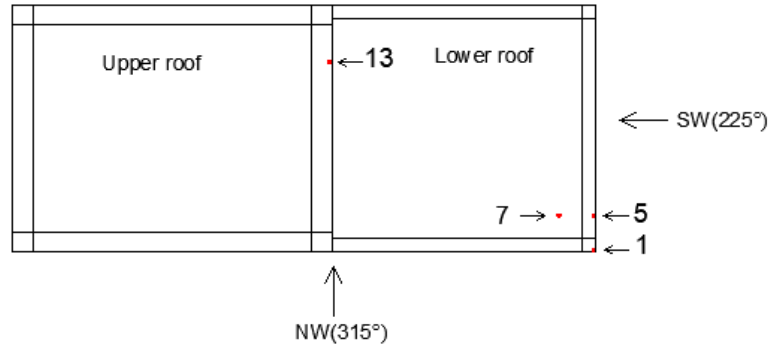


Figure 11: Comparison of field and experimental negative peak and mean pressure coefficients in the lower corner zone (tap 1), Lower edge zone (tap 5), lower interior zone (tap 7), and upper edge (tap 13).

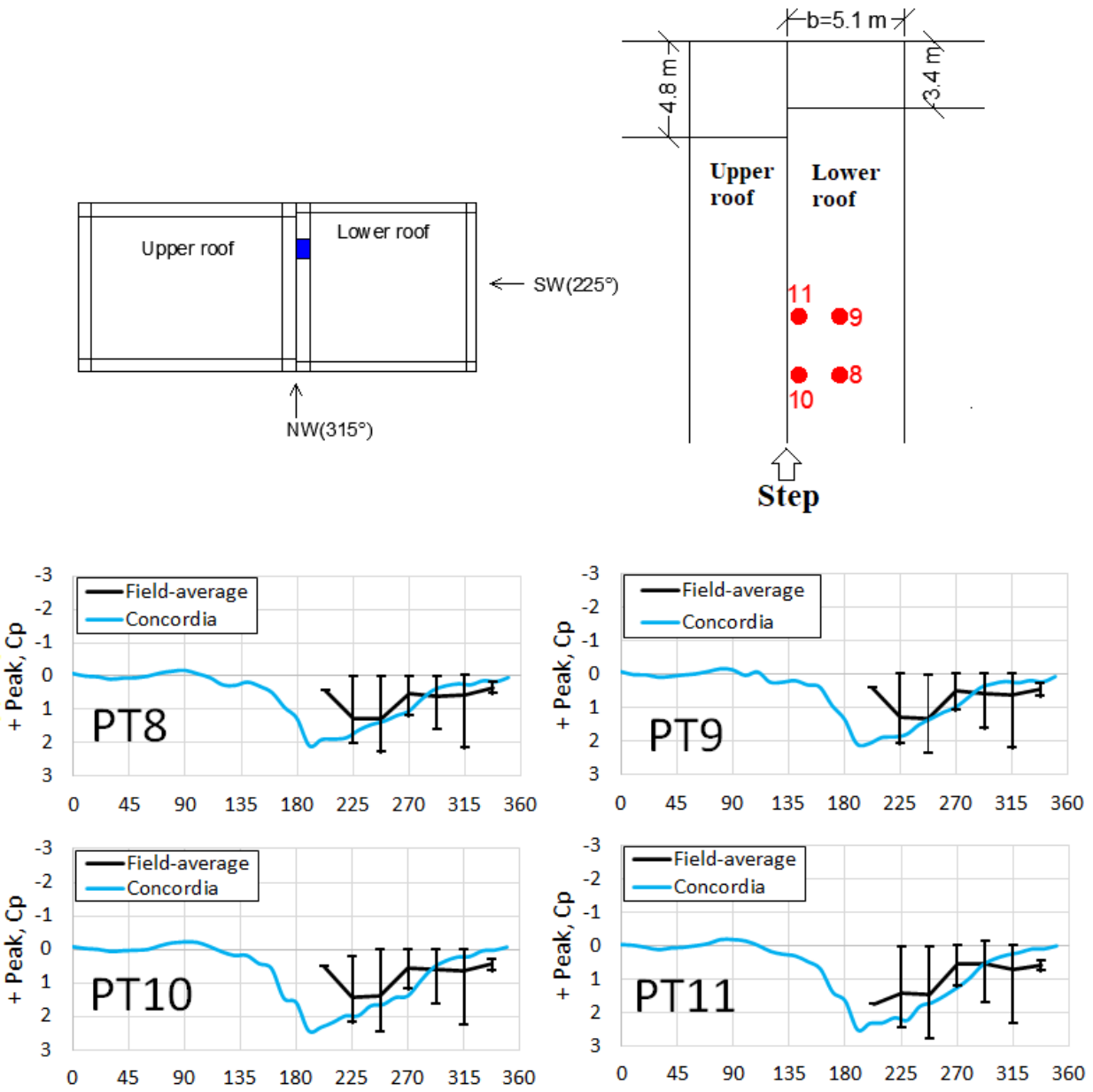


Figure 12: Comparison of field and experimental positive peak pressure coefficients in the positive pressure zone on the lower roof near the step.

Table 1: Comparison of most critical pressure coefficients between field, Concordia, and Stathopoulos and Luchian (1990)

	Field		Concordia		Stathopoulos and Luchian (1990)	
	Mean	Peak (-)	Mean	Peak (-)	Mean	Peak (-)
Lower corner	-3.2	-8.4	-2.2	-6.2	-1.6	-4.2
Lower edge	-2	-4.1	-1.6	-4.5	-0.8	-2.8
Lower interior	-1.4	-4.6	-0.9	-2.9	-0.5	-2.5
Upper edge	-1.9	-4.5	-1.6	-5	-1.1	-3

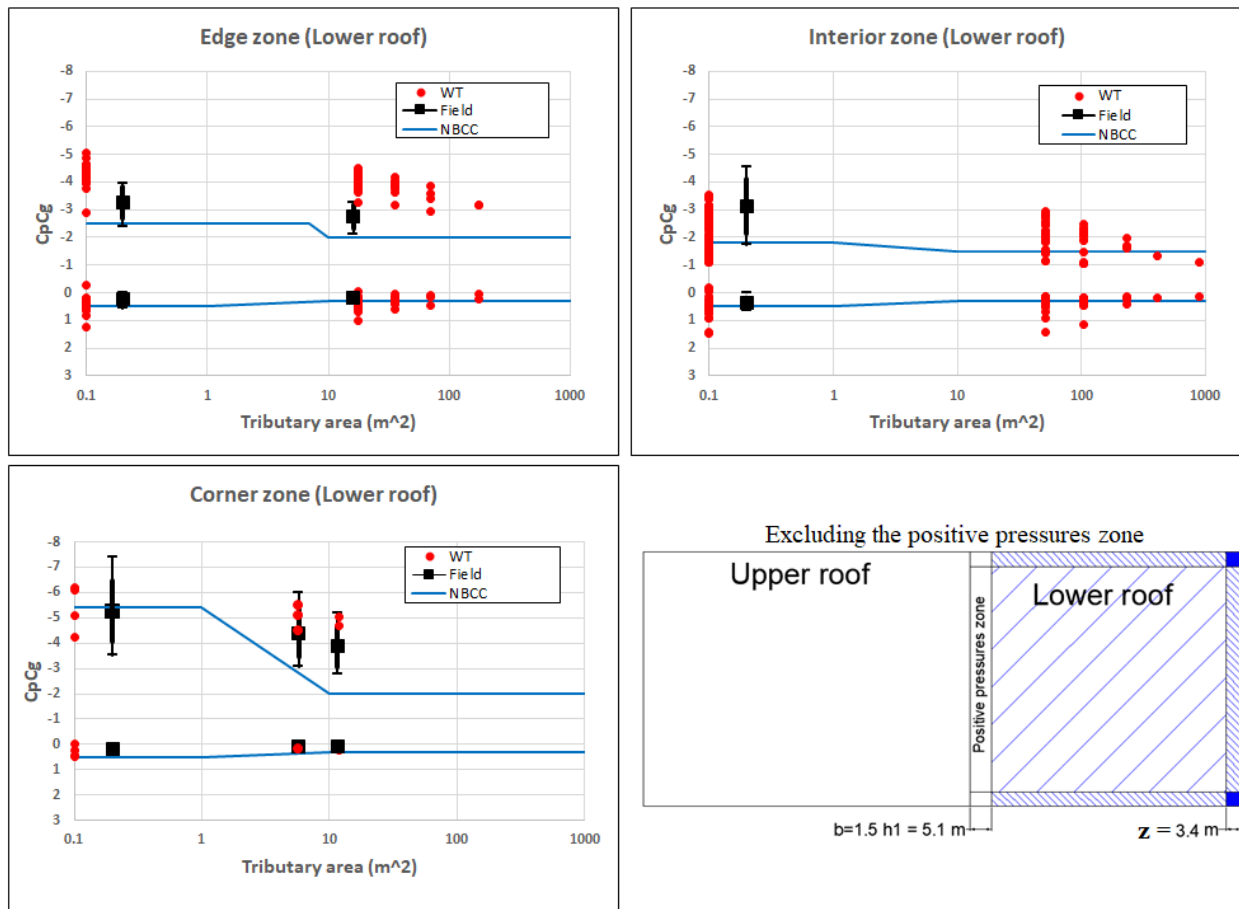


Figure 13: Comparison of the enveloped experimental peaks of the lower roof with field peaks and the corresponding recommendation of NBCC 2020 in the corner, edge, and interior zones (excluding the positive pressure zone).

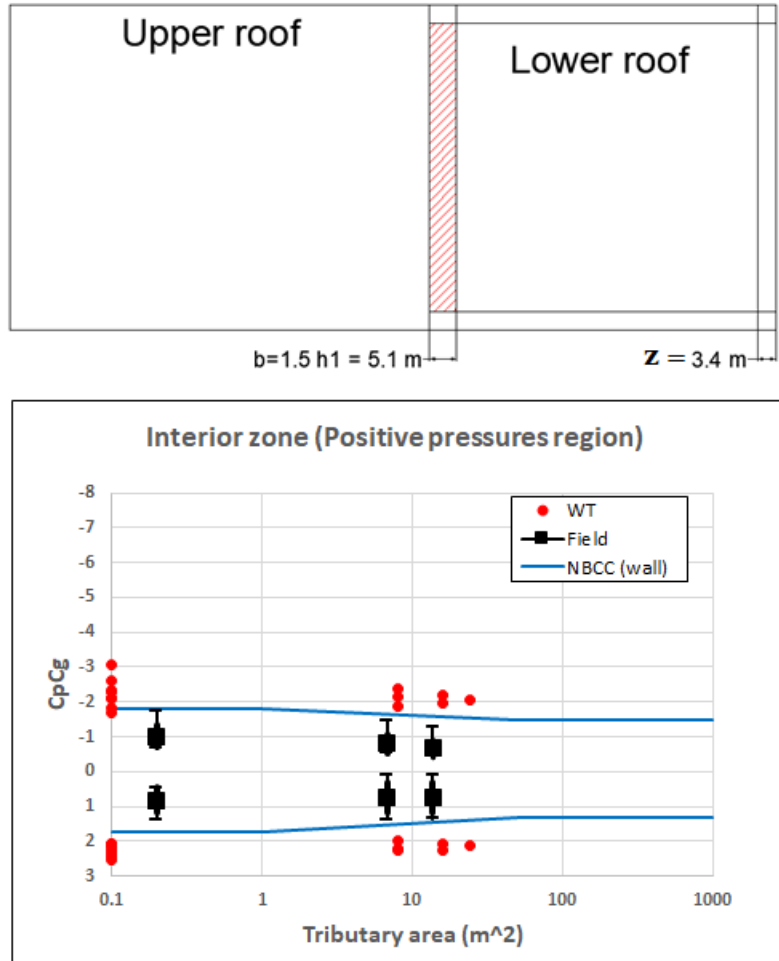


Figure 14: Comparison of the enveloped experimental peaks of the positive pressure zone with field peaks and the corresponding recommendation of NBCC 2020 in the interior zones.

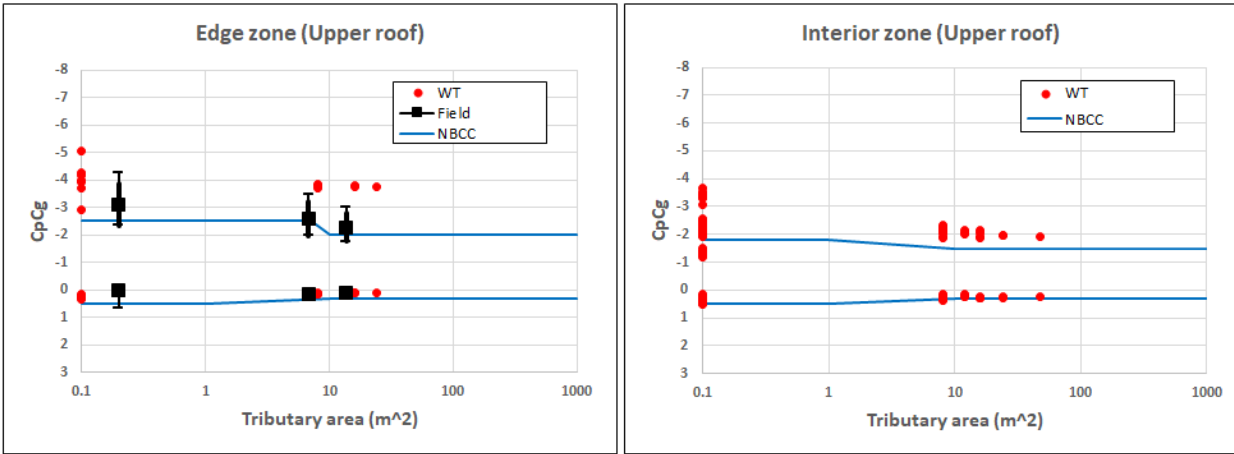
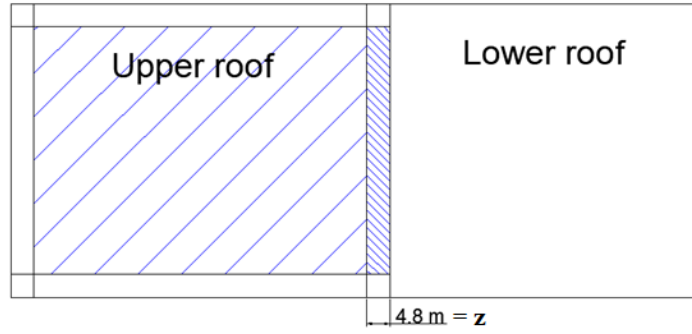


Figure 15: Comparison of the enveloped experimental peaks of the upper roof with the field peaks and the corresponding recommendation of NBCC 2020 in the edge and interior zones.

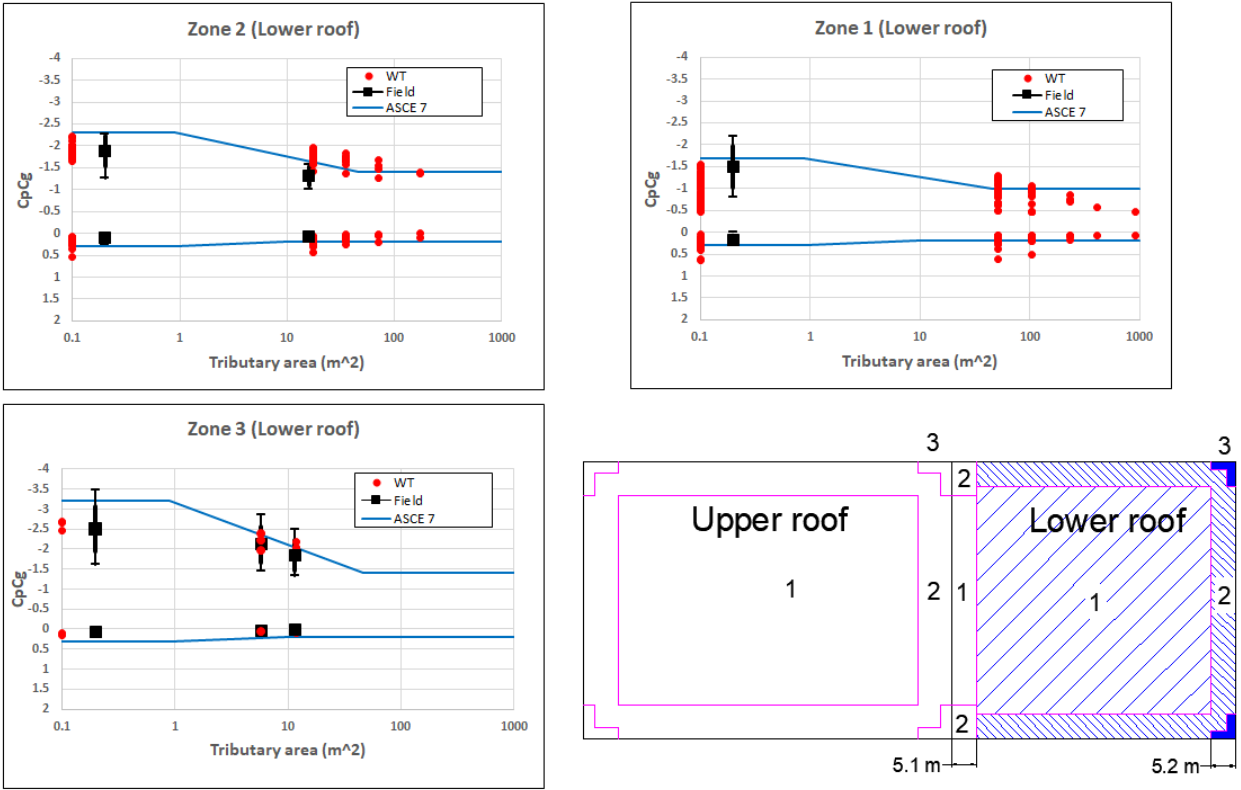


Figure 16: Comparison of the enveloped experimental peaks of the lower roof with field peaks and the corresponding peaks of ASCE 7-22 in Zone 3, Zone 2, and Zone 1.

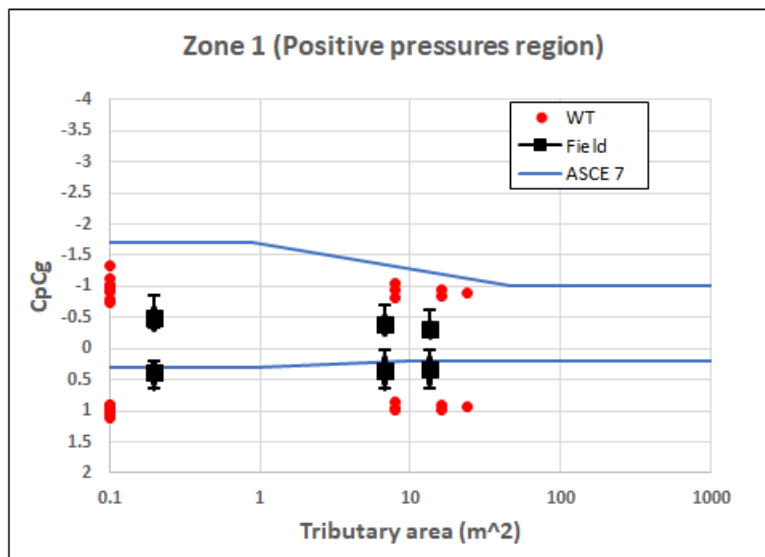
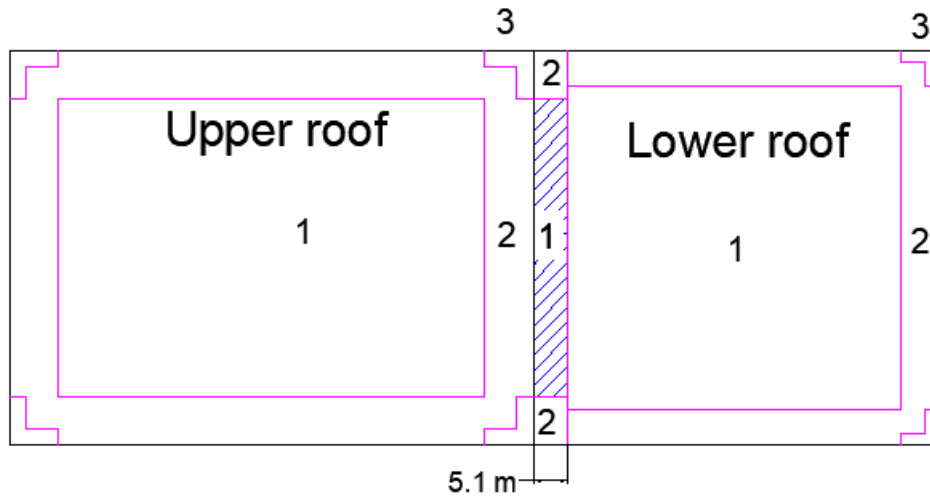


Figure 17: Comparison of the enveloped experimental peaks of Zone 1 (near the step wall) with field peaks and the corresponding peaks of ASCE 7-22.

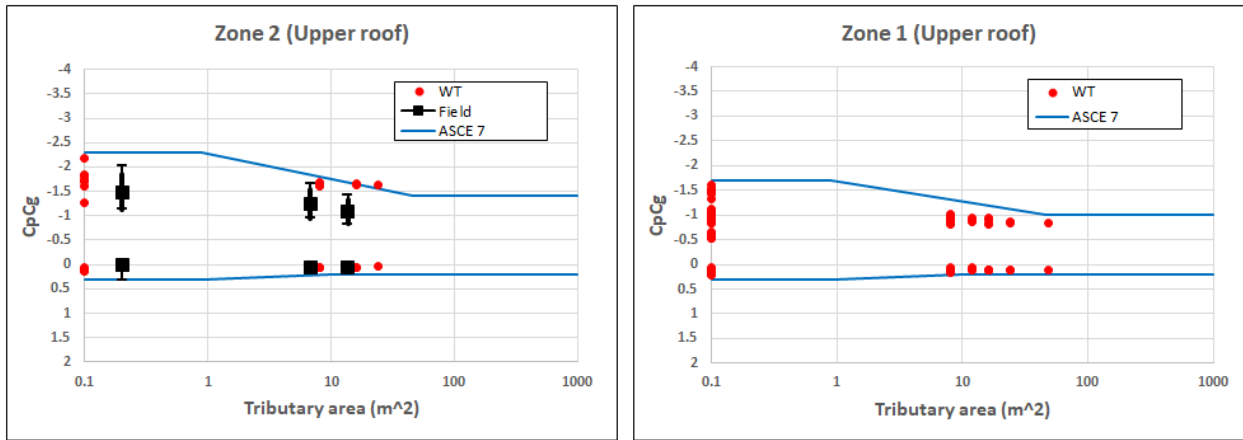
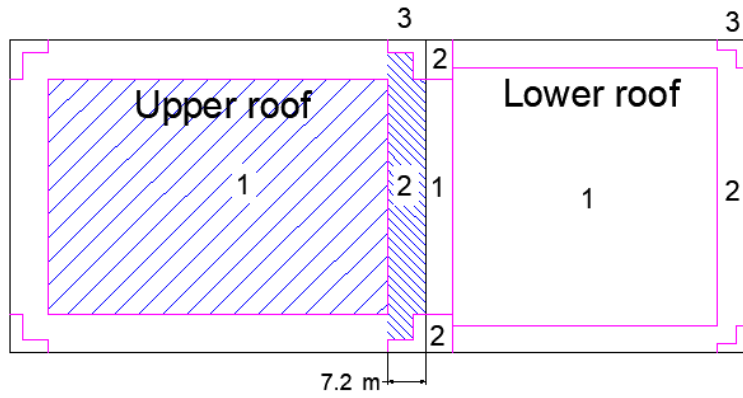


Figure 18: Comparison of the enveloped experimental peaks of the upper roof with field peaks and the corresponding peaks of ASCE 7-22 in Zone 2 and Zone 1.